Brief Report

Determination of Electronic Loss in Cu(In,Ga)Se2 Solar Cell by Spectroscopic Ellipsometry Analysis and External Quantum Efficiency Simulation

Dhurba R. Sapkota * and Rabee B. Alkhayat

Posted Date: 17 May 2023

doi: 10.20944/preprints202305.1203.v1

Keywords: CIGS; SE measurement; Device Analysis; EQE simulation

Article

Determination of Electronic Loss in Cu(In,Ga)Se_2 Solar Cell by Spectroscopic Ellipsometry Analysis and External Quantum Efficiency Simulation

Dhurba R. Sapkota [1] and Rabee B. Alkhayat [2]

[1] Wright Center for Photovoltaics Innovation & Commercialization, Univ of Toledo, Toledo, Ohio 43606, USA

[2] Department of Physics, College of Education for Pure Science, Univ of Mosul, 41002 Iraq

Abstract: Copper indium gallium diselenide, Cu(In,Ga)Se_2, thin-film of about 1.2 μm has been deposited on Mo coated soda lime glass by thermal co-evaporation of Cu, In, Ga, and Se sources. The thin film CIGS was characterized by energy dispersive spectroscopy (EDS) and identified the elemental composition of Cu, In, Ga and Se in the film. A CIGS device was completed by the successive deposition of multiple layers; SLG/Mo/CIGS/CdS/ZnO/ITO which yielded the efficiency of 11%. External spectroscopic ellipsometry (ex-situ SE) was performed on the completed device and the device analysis was performed. Starting with the parameterized complex dielectric functions of the individual component layers, SE analysis was performed using a step-wise procedure that ranks the fitting parameters according to their ability to reduce the mean square error (MSE) of the fit. The resulting layer thicknesses and dielectric functions were used to simulate the external quantum efficiency (EQE) of the device assuming complete active layer collection. Electronic losses were identified by comparison of simulated EQE with the measured EQE. The ultimate goal of this work is the optimization of narrow band-gap CIGS-related solar cells for the bottom layer in tandem devices.

Keywords: CIGS; SE measurement; Device Analysis; EQE simulation

1. Introduction

Cu (In_{1-x},Ga_x) Se_2 (CIGS with x = Ga/In+Ga) as a good photovoltaic absorber has attracted interest since the first report as a CIS (x = 0) by Wagner et al. in 1974. In this report fabrication of a hetero-junction CIS/CdS PV detector using a bulk p-type crystalline CIS absorber that yielded a solar conversion efficiency of 5% [1,2]. The CIGS efficiency is optimized at x ∽ 0.3[3] and decreased with x > 0.3 [3,4]. The first fully thin film $CuInSe_2$/CdS solar cells were fabricated from absorbers co-evaporated from $CuInSe_2$ and Se in a single stage [5]. Series of CIS device optimization and characterizations were presented previously [6–8] and this research is the continuation of CIS and adding Ga to convert into CIGS. CIGS has attracted great interest as an absorber layer in the field of thin film solar cells due to its high efficiency over the time[3,9–14]. Jackson et al. reported the CIGS with the efficiencies 21.7 % and 22.6% in 2015 and 2016 respectively[14,15]. Cadmium free CIG (Se, $S)_2$ with the conversion efficiency of 23.35% was reported in 2019 by Nakamura et al. [16]. The potential alternatives of CdS for the fabrication of Cd free CIGS would be the magnesium zinc oxide (MZO) and indium gallium oxide (IGO), the details of their properties were studied [17,18].

Researchers are focused on CIGS thin films due to their potential application in multijunction perovskite tandem solar cells. The band gap ∽1.20 eV of CIGS is well- suited for this application along with its favorable electronic properties and controllable p-type conductivity. CIGS is a chalcopyrite compound alloy with a direct bandgap and an optical absorption coefficient greater than 10^5 cm−1 above the bandgap. Due to its thermal and chemical stability, adjustability of its bandgap by adjusting the gallium content, low light degradation, and high stability under high energy irradiation, CIGS has been one of the most promising absorber materials for thin film solar cells. If the Ga content x = Ga /In + Ga in the CIGS is reduced to zero, the result is the CIS ternary compound with a direct bandgap of ∽ 1.02 eV. The bandgap energy can be increased by adding Ga to CIS and

Preprints (www.preprints.org) | NOT PEER-REVIEWED | Posted: 17 May 2023 doi:10.20944/preprints202305.1203.v1

converting it to CIGS CIS. This work focuses on procedure for the understanding of the carrier collection and electronic loss for a CIGS (x = 0.3) device via spectroscopic ellipsometry (SE) analysis, external quantum efficiency measurement and simulation. Previously a similar study was made and presented for the CIS device (CIGS: x = 0.0) [19]. Study of degradation of CIGS, the optical properties and band gap of CIS/CIGS and Urbach tail energies were presented previously[7,20] and these results were applied to design the perovskite tandems [21,22]. Before studying CIGS, several studies were made for the CIS (CIGS: x = 0.0) including optical hall effect, structural and optical studies, device simulation and characterizations by different methods[6–8,23–28].

2. Experimental Details

CIGS device was completed by the deposition of different layers in sequence starting from the Mo back contact and ending with metal grid as shown in the Fig 1. Soda lime glass (SLG) of 2.5 cm × 7.5 cm × 0.15 cm in size was used as a substrate. Bared SLG were first cleaned using micro-90 solution, followed by rinsing in deionized water in an ultrasonic cleaner and then dried with nitrogen gas. Cleaned SLG were immediately put inside the vacuum chamber for the Mo deposition. Mo ∽0. 6 µm was deposited on Soda-lime glass (SLG) by DC sputtering at 250°C by two-step sputtering process. Deposition and process parameters play a major role in achieving the appropriate properties for a layer [29]. Mo coated SLG was then transferred to the thermal co-evaporation chamber for the absorber layer (CIGS) deposition. CIGS ∽1.2 µm was deposited on top of Mo by one stage thermal co-evaporation procedure keeping the substrate at 570°C during the deposition. One stage thermal co-evaporation process was performed in a high vacuum chamber by evaporating the corresponding elements Cu, In, Ga, Se at same time by adjusting the source temperature to maintain the CIGS deposition rate of ∽7-8 Å/s. Buffer layer CdS ∽ 0.05 µm was deposited on top of CIGS by chemical bath deposition procedure. Most efficient CIGS-based solar cells have been prepared using CdS as the n-type buffer layer. In this process, an aqueous solution of cadmium acetate and thiourea with ammonium hydroxide catalyst was used [28]. A bi-layer of transparent conductive oxide i-ZnO followed by Indium-dopped tin oxide ITO was deposited on top of CdS. This front contact layer was deposited with intended thickness of 0.05/0.2 µm by RF sputtering in high vacuum by keeping the sample at room temperature. Immediately it was followed by the metal grid deposition of tri layer Ni/Al/Ni by electron beam evaporation.

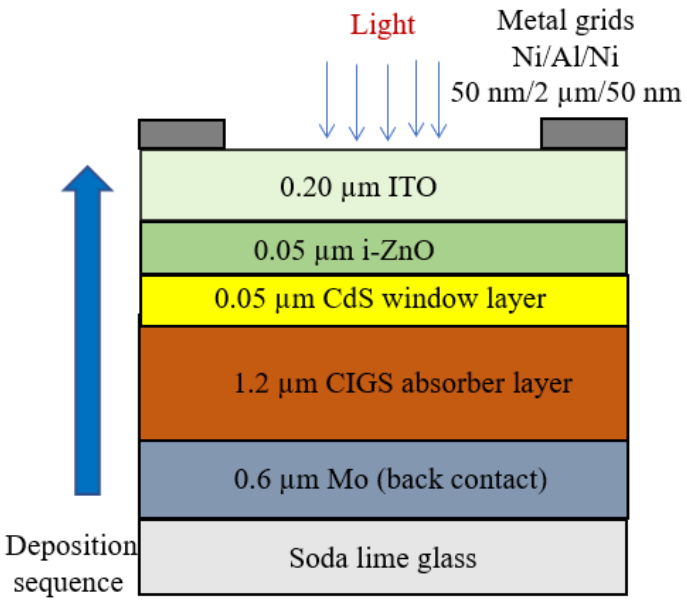

Figure 1. Schematic of the CIS solar cell structure in the substrate configuration used in this study.

Preprints (www.preprints.org) | NOT PEER-REVIEWED | Posted: 17 May 2023 doi:10.20944/preprints202305.1203.v1

2.1. SE Analysis and EQE SIMULATION

Ellipsometry is an optical technique traditionally used for measuring the thickness and investigating the dielectric properties, i.e., the complex index of refraction or complex dielectric function, of thin films and stack layers. Spectroscopic ellipsometry (SE) involves performing the ellipsometry measurement continuously versus source wavelength and, over the years, has become a powerful non-contacting and non-invasive optical technique for the characterization of materials of different kind. In a SE measurement, one determines as a function of incident beam wavelength the change of polarization upon reflection from or transmission through one or more interfaces that comprise the sample structure. During the model analysis; this measured change is compared to that simulated using structural and optical models of the sample. The models are then adjusted to fit the measured result. SE technique can be used to characterize material structure including thicknesses and surface morphologies. SE is a powerful tool which be used to extract optical properties, the real and imaginary parts the complex dielectric function (ε_1, ε_2) as a function of incident photon energy.

To explore the limitations on single stage CIGS solar cell efficiency the EQE spectrum has been modelled. EQE simulation was performed by measuring the SE on whole device and extracting the complex dielectric functions (ε_1, ε_2) of the component layers used in the actual device as in Fig 1.A step wise reduction of mean square error (MSE) procedure as presented in Figure 2 was applied while performing the device analysis with best fitting of actual data with SE model [19,28]. SE measurement was performed on the CIGS solar cell at a 50^0 angle of incidence with in the photon energy range of 0.73 eV to 4.0 eV. SE data were fitted using a multilayer model including structural and optical properties as presented in Table I. The SE data were fitted by using multilayer stack of device structure. This multilayer stack also includes layer volume fractions which control the (ε_1, ε_2) spectra, were determined in a step-wise MSE reduction procedure. Each fitting parameter of the model was ordered in two sets according to its ability to reduce the MSE, the first set structural parameters and the second set optical property parameters [30]. The MSE reduction procedure in which case the square root of the MSE is given in terms of the Muller matrix spectra (N, C, S) as

$$\sigma_{NCS} = \sqrt{\frac{1}{3n-p}\sum_{i=1}^{n}\left[\left(\frac{N_i^{(e)}-N_i^{(c)}}{\sigma_{N,i}^{(e)}}\right)^2+\left(\frac{C_i^{(e)}-C_i^{(c)}}{\sigma_{C,i}^{(e)}}\right)^2+\left(\frac{S_i^{(e)}-S_i^{(c)}}{\sigma_{S,i}^{(e)}}\right)^2\right]}.$$

In this equation, n is the number of spectral points and p is the number of fitting parameters. The superscripts (e) and (c) represent experimental and calculated values of $N = \cos2\psi$, $C = \sin2\psi\cos\Delta$, and $S = \sin2\psi\sin\Delta$. The quantities $\sigma_{j,i}$ are estimates of the errors in $j = N, C, S$, at spectral position i for the ellipsometer used in this study. The results of the procedure from which nine structural and eight optical property parameters deduced are presented in Table I and Figure 2. From the final best fit spectra in the ellipsometry angles (ψ, Δ), the Mueller matrix spectra $N = \cos2\psi$, $C = \sin2\psi\cos\Delta$, and $S = \sin2\psi\sin\Delta$ spectra (lines) can be determined as shown along with the data (points) in Figure 3.

Preprints (www.preprints.org) | NOT PEER-REVIEWED | Posted: 17 May 2023 doi:10.20944/preprints202305.1203.v1

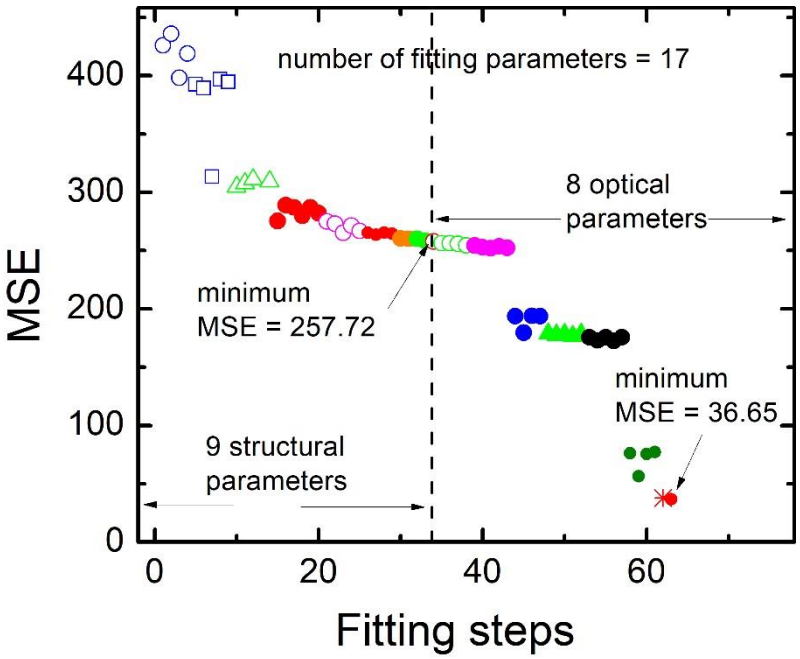

Figure 2. Step-wise mean square error reduction in the analysis of SE data collected from the CIGS solar cell at an angle of incidence of 50°.

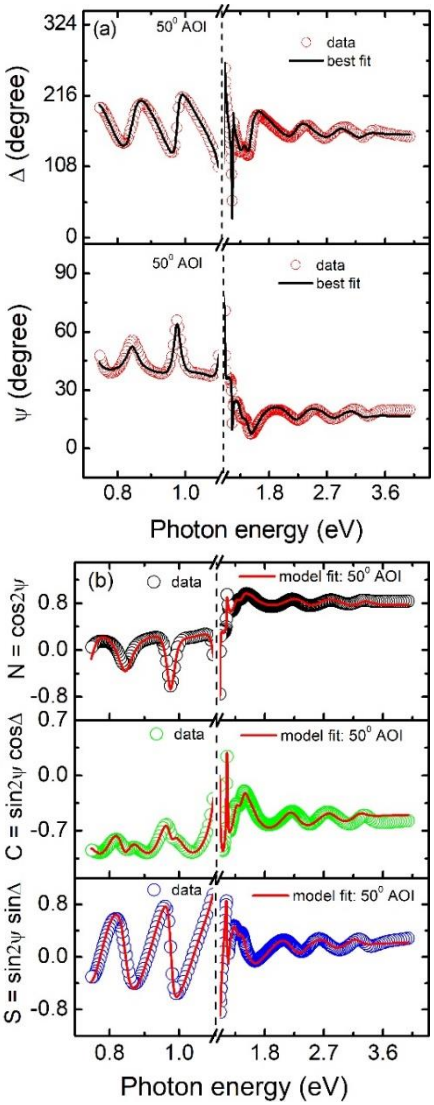

 doi:10.20944/preprints202305.1203.v1

Figure 3. (a) (ψ, Δ) best fit matching of model and data, (b) experimental Mueller matrix spectra (*N*, *C*, *S*) from a spectroscopic ellipsometry measurement of the CIGS solar cell along with the corresponding best fit results using the model of Figure 4.

Table I was utilized to simulate and model the External quantum efficiency (EQE) of the device. CIGS and CIGS/CdS interface layers are the active layers which contribute to the photogenerated charge carrier collection as presented in the Figure 5. Figure 6 shows the measured normal incidence EQE spectrum, along with the summed spectrum from Figure 5 simulated assuming 100% contribution from the two active layers. The reflectance of the complete multilayer structure and the optical absorption of each layer in the structure of the CIGS cell obtained via simulation are presented in Figure 7. Presented in the Figure 8 is a comparison of the measured complex dielectric functions spectra of the CIGS device obtained before (individual layers) and after from device analysis.

Layer (composition, properties)	Thickness	Effective thickness
surface roughness (f_v = 28.9 ± 0.5 %)	35.4 ± 0.5 nm	
ITO (f_v = 0 %)	104.1 ± 3.4 nm	ITO: 150 nm
i-ZnO /ITO (f_{ZnO} = 50 %)	39.8 ± 3.8 nm	
i-ZnO (f_v = 0 %)	30.0 ± 7.4 nm	i-ZnO: 74 nm
CdS / i-ZnO (f_{CdS} = 50 %)	47.2 ± 2.4 nm	
CdS (f_v = 0 %)	32.6 ± 6.5 nm	CdS: 77 nm
CIGS / CdS (f_{CIGS} = 64.6 ± 0.1 %)	59.1 ± 1.8 nm	
CIGS (f_v = 0 %)	1138.2 ± 6.7 nm	CIGS: 1179 nm
Mo / CIGS (f_{Mo} = 92.4 ± 1.2 %)	38.2 ± 4.4 nm	
Mo (opaque)		Mo

Figure 4. Layer stack of the CIGS solar cell including bulk, interface, and surface layers from the SE analysis of Figures 2 and 3, and Table I.

Preprints (www.preprints.org) | NOT PEER-REVIEWED | Posted: 17 May 2023 doi:10.20944/preprints202305.1203.v1

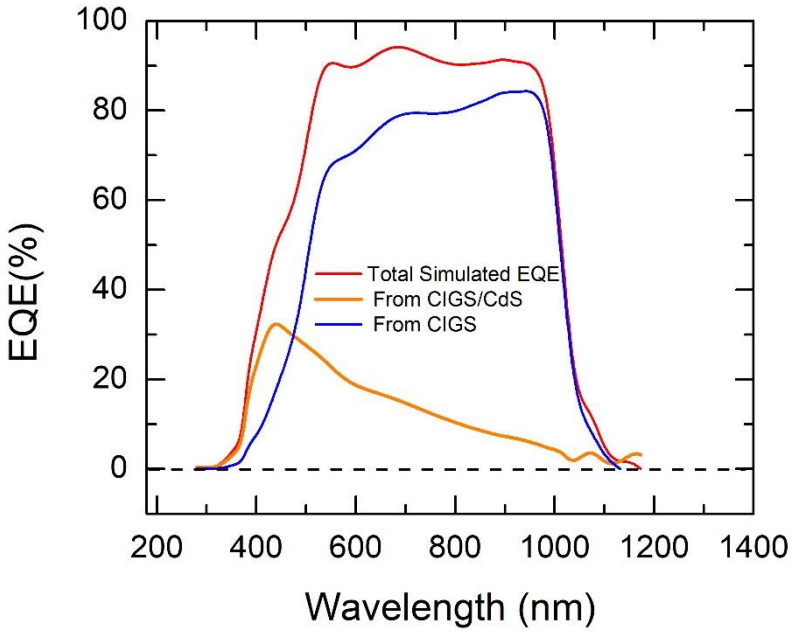

Figure 5. Components of the EQE spectrum from the two active layers of the CIGS solar cell structure of Figure 4 simulated optically assuming 100% charge carrier collection.

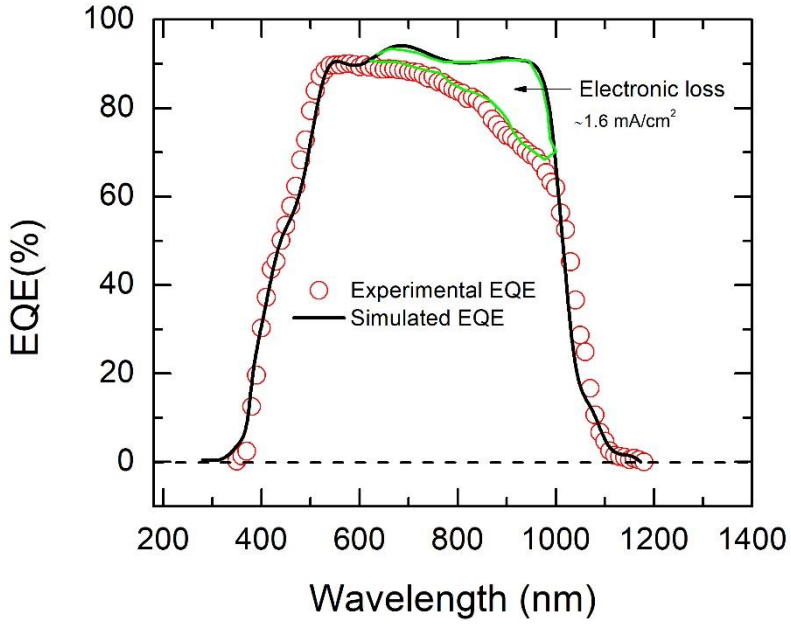

Figure 6. Measured normal incidence EQE and the ideal simulated EQE (black line) of thin film CIGS. Electronic loss was obtained from simulation by using the structural model and complex dielectric functions as presented in Figs.4 and 9.

Preprints (www.preprints.org) | NOT PEER-REVIEWED | Posted: 17 May 2023 doi:10.20944/preprints202305.1203.v1

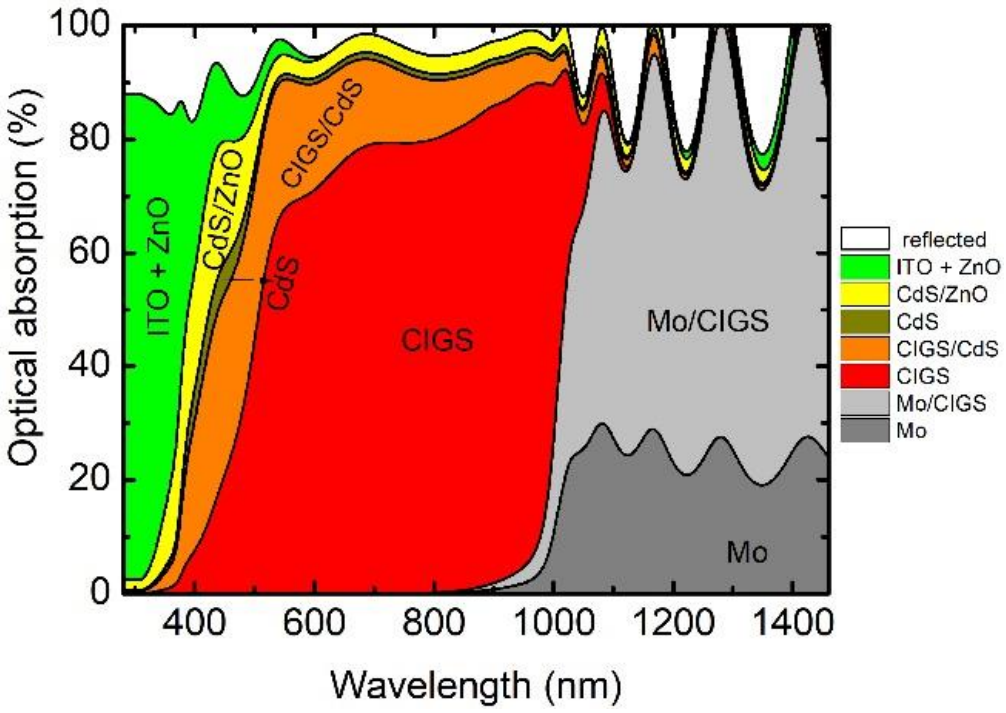

Figure 7. Simulated reflectance from the complete stack and optical absorption in the individual layers of the CIS solar cell structure.

A set of complex dielectric functions (ε_1, ε_2) was determined applying ex-situ spectroscopic ellipsometry measurements and analyses of the component layers used in the CIGS device. These complex dielectric functions were utilized for SE analysis of the complete CIGS solar cell in order to extract photon energy independent structural and optical property parameters that enable simulation of the external quantum efficiency (EQE). Considering the Mo back contact layer first, there have been no changes in the deposition chamber and procedure other than standard maintenance since the previous optical study by Pradhan [28,31]. As a result, the complex dielectric function of Mo obtained by in-situ SE from the previous work were utilized in this work [31]. The (ε_1, ε_2) spectra of the CIGS absorber layer were utilized from the previous study of CIGS from the same chamber and deposition procedures [32]. The spectra CdS, ZnO, and ITO were determined in the present work utilizing ex-situ SE measurement and data analysis methods. To extract the complex dielectric functions, samples in this study were deposited on native oxide coated Si wafers, and all data were analyzed using the structural model presented in Fig 8. The complex dielectric function of the surface roughness layer in Figure 8 was modeled using the Bruggeman effective medium approximation (EMA) by assuming a mixture consisting of bulk layer material and voids characterized in terms of their volume percentages[33].

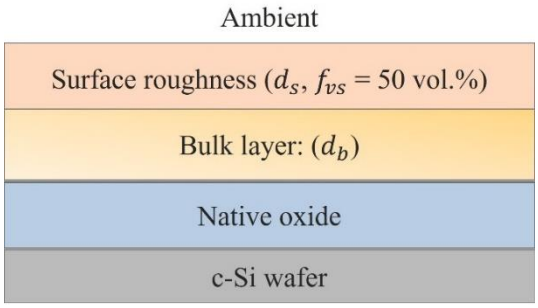

Figure 8. Model used in the SE study of the thin film component layers of the CIGS solar cell including CdS, ZnO, and ITO, each deposited on a c-Si wafer substrate. Variable structural parameters include the bulk layer thickness d_b, and the surface roughness layer thickness d_s [28].

Preprints (www.preprints.org) | NOT PEER-REVIEWED | Posted: 17 May 2023 doi:10.20944/preprints202305.1203.v1

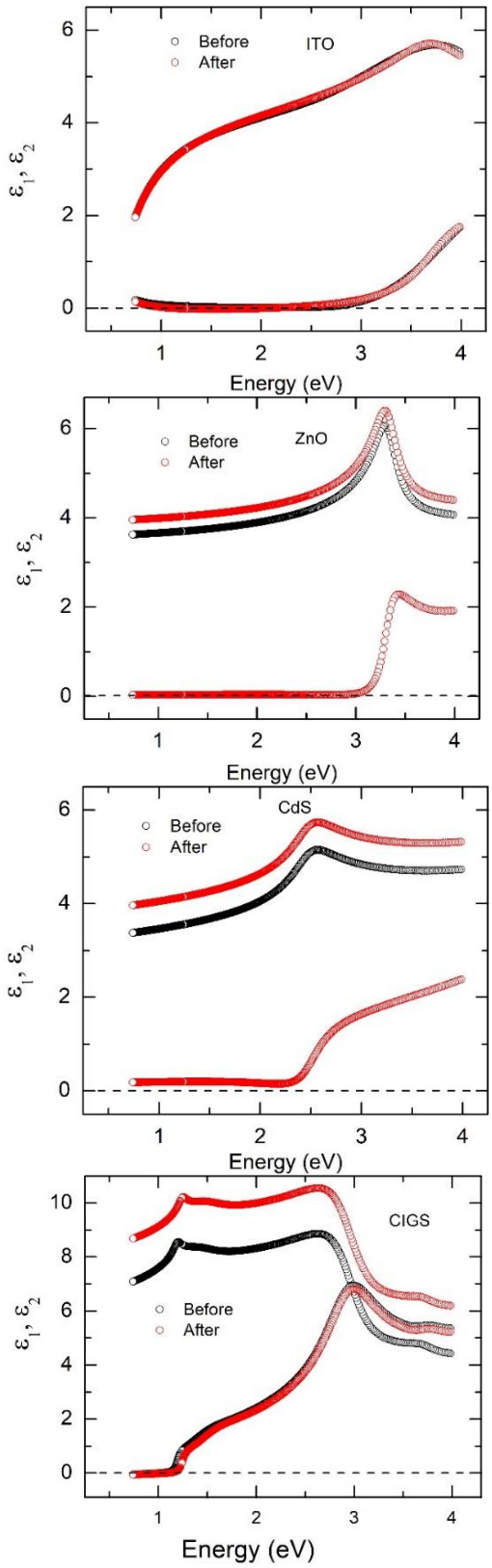

Figure 9. Complex dielectric functions of the component layers before device fabrication and obtained from the device.

3. Conclusion

Multilayer structural analysis by SE on thin film CIGS solar cell by spectroscopic ellipsometry (SE) is performed. Complex dielectric functions layers from the CIGS stack layers were utilized for the EQE simulation and compared with measured results. Observed deviation is utilized to refine the

optical model for the cell, as well as to identify electronic losses in the present configuration and deposition procedures of the layer stack. Complete collection by the active layers CIGS/CdS interface and CIGS absorber layers, was expected to yield a potential short circuit current density of 32.44 mA/cm^2 as obtained from simulation. The lower experimental value of J_{sc} = 30.87 mA/cm^2 is an indication of recombination in the absorber layer along with possible effects of a large conduction band offset at the CdS/CIGS interface and this also indicates the formation of barrier against collection of the photogenerated electrons in the absorber [30]. Total of $\backsim$ 1.6 mA/cm^2 loss is identified from the experimental and simulated EQE comparison. Study of change in complex dielectric functions of the component layers deposited separately and in stack on top of each other is presented. Future steps will involve optimization of the CIGS performance by reducing the deep absorber recombination and top contact optical losses through variations in the CIGS thickness and other layer thicknesses of the device.

ACKOWLEDGEMENT: Department of Physics, College of Education for Pure Science, Univ of Mosul, 41002 Iraq. Wright Center for Photovoltaics Innovation & Commercialization, University of Toledo, Toledo, Ohio, 43606, USA.

References

1. Wagner, S.; Shay, J.; Migliorato, P.; Kasper, H. CuInSe$_2$/CdS heterojunction photovoltaic detectors. *Applied Physics Letters* **1974**, *25*, 434-435.
2. Shay, J.; Wagner, S.; Kasper, H. Efficient CuInSe$_2$/CdS solar cells. *Applied Physics Letters* **1975**, *27*, 89-90.
3. Shafarman, W.N.; Klenk, R.; McCandless, B.E. Device and material characterization of Cu (InGa) Se2 solar cells with increasing band gap. *Journal of Applied Physics* **1996**, *79*, 7324-7328.
4. Ramanathan, K.; Contreras, M.A.; Perkins, C.L.; Asher, S.; Hasoon, F.S.; Keane, J.; Young, D.; Romero, M.; Metzger, W.; Noufi, R. Properties of 19.2% efficiency ZnO/CdS/CuInGaSe$_2$ thin-film solar cells. *Progress in Photovoltaics: research and applications* **2003**, *11*, 225-230.
5. Kazmerski, L.; White, F.; Morgan, G. Thin-film CuInSe$_2$/CdS heterojunction solar cells. *Applied Physics Letters* **1976**, *29*, 268-270.
6. Sapkota, D.R.; Pradhan, P.; Koirala, P.; Irving, R.; Phillips, A.B.; Ellingson, R.J.; Heben, M.J.; Marsillac, S.; Podraza, N.J.; Collins, R.W. Structural and Optical Properties of Two-Stage CuInSe$_2$ Thin Films Studied by Real Time Spectroscopic Ellipsometry. In Proceedings of 2019 IEEE 46th Photovoltaic Specialists Conference (PVSC), 16-21 June 2019; pp. 0943-0948.
7. Sapkota, D.R.; Koirala, P.; Pradhan, P.; Shrestha, N.; Junda, M.M.; Phillips, A.B.; Ellingson, R.J.; Heben, M.J.; Marsillac, S.; Podraza, N.J. Spectroscopic Ellipsometry Investigation of CuInSe$_2$ as a Narrow Bandgap Component of Thin Film Tandem Solar Cells. In Proceedings of 2018 IEEE 7th World Conference on Photovoltaic Energy Conversion (WCPEC)(A Joint Conference of 45th IEEE PVSC, 28th PVSEC & 34th EU PVSEC); pp. 1943-1948.
8. Sapkota, D.; Koirala, P.; Pradhan, P.; Collins, R. Real Time Spectroscopic Ellipsometry Analysis of the Structural Evolution and Optical Properties of CuInSe$_2$. *Bulletin of the American Physical Society* **2018**, *63*.
9. Repins, I.; Contreras, M.A.; Egaas, B.; DeHart, C.; Scharf, J.; Perkins, C.L.; To, B.; Noufi, R. 19· 9%-efficient ZnO/CdS/CuInGaSe$_2$ solar cell with 81· 2% fill factor. *Progress in Photovoltaics: Research and applications* **2008**, *16*, 235-239.
10. Shafarman, W.N.; Siebentritt, S.; Stolt, L. Cu(In,Ga)Se$_2$ Solar Cells. *Handbook of photovoltaic science and engineering* **2010**, 546-599.
11. Jackson, P.; Hariskos, D.; Lotter, E.; Paetel, S.; Wuerz, R.; Menner, R.; Wischmann, W.; Powalla, M. New world record efficiency for Cu(In,Ga)Se$_2$ thin-film solar cells beyond 20%. *Progress in Photovoltaics: Research and Applications* **2011**, *19*, 894-897.
12. Chirilă, A.; Buecheler, S.; Pianezzi, F.; Bloesch, P.; Gretener, C.; Uhl, A.R.; Fella, C.; Kranz, L.; Perrenoud, J.; Seyrling, S. Highly efficient Cu(In,Ga)Se$_2$ solar cells grown on flexible polymer films. *Nature materials* **2011**, *10*, 857-861.
13. Jackson, P.; Hariskos, D.; Wuerz, R.; Wischmann, W.; Powalla, M. Compositional investigation of potassium doped Cu(In,Ga)Se$_2$ solar cells with efficiencies up to 20.8%. *physica status solidi (RRL)–Rapid Research Letters* **2014**, *8*, 219-222.

14. Jackson, P.; Wuerz, R.; Hariskos, D.; Lotter, E.; Witte, W.; Powalla, M. Effects of heavy alkali elements in Cu(In,Ga)Se_2 solar cells with efficiencies up to 22.6%. *physica status solidi (RRL)–Rapid Research Letters* **2016**, *10*, 583-586.
15. Jackson, P.; Hariskos, D.; Wuerz, R.; Kiowski, O.; Bauer, A.; Friedlmeier, T.M.; Powalla, M. Properties of Cu(In,Ga)Se_2 solar cells with new record efficiencies up to 21.7%. *physica status solidi (RRL)–Rapid Research Letters* **2015**, *9*, 28-31.
16. Nakamura, M.; Yamaguchi, K.; Kimoto, Y.; Yasaki, Y.; Kato, T.; Sugimoto, H. Cd-free Cu(In,Ga)$(Se,S)_2$ thin-film solar cell with record efficiency of 23.35%. *IEEE Journal of Photovoltaics* **2019**, *9*, 1863-1867.
17. Alaani, M.A.R.; Koirala, P.; Phillips, A.B.; Liyanage, G.K.; Awni, R.A.; Sapkota, D.R.; Ramanujam, B.; Heben, M.J.; O'Leary, S.K.; Podraza, N.J. Optical Properties of Magnesium-Zinc Oxide for Thin Film Photovoltaics. *Materials* **2021**, *14*, 5649.
18. Jamarkattel, M.K.; Phillips, A.B.; Subedi, I.; Abudulimu, A.; Bastola, E.; Li, D.-B.; Mathew, X.; Yan, Y.; Ellingson, R.J.; Podraza, N.J. Indium Gallium Oxide Emitters for High-Efficiency CdTe-Based Solar Cells. *ACS Applied Energy Materials* **2022**.
19. Sapkota, D.R.; Shan, A.; Ramanujam, B.; Pradhan, P.; Irving, R.; Phillips, A.B.; Heben, M.J.; Ellingson, R.J.; Marsillac, S.; Podraza, N.J. Spectroscopic Ellipsometry Analysis and Quantum Efficiency Simulation of CuInSe 2 Solar Cells. In Proceedings of 2022 IEEE 49th Photovoltaics Specialists Conference (PVSC); pp. 0407-0412.
20. Alkhayat, R.B.; Sapkota, D.R. Study of Degradation of Cu (In, Ga) Se 2 Solar Cell Parameters due to Temperature. In Proceedings of 2022 IEEE 49th Photovoltaics Specialists Conference (PVSC); pp. 1252-1256.
21. Ahangharnejhad, R.H.; Song, Z.; Phillips, A.B.; Watthage, S.C.; Almutawah, Z.S.; Sapkota, D.R.; Koirala, P.; Collins, R.W.; Yan, Y.; Heben, M.J. Optical design of perovskite solar cells for applications in monolithic tandem configuration with CuInSe2 bottom cells. *MRS Advances* **2018**, *3*, 3111-3119.
22. Hosseinian Ahangharnejhad, R.; Song, Z.; Phillips, A.; Watthage, S.; Almutawah, Z.; Sapkota, D.R.; Koirala, P.; Collins, R.; Yan, Y.; Heben, M. Optical design of perovskite solar cells for applications in tandem configuration with CuInSe$_2$ bottom cells. *Bulletin of the American Physical Society* **2018**, *63*.
23. Shrestha, N.; Sapkota, D.R.; Subedi, K.K.; Pradhan, P.; Koirala, P.; Phillips, A.B.; Collins, R.W.; Heben, M.J.; Ellingson, R.J. Identification of defect levels in copper indium diselenide ($CuInSe_2$) thin films via photoluminescence studies. *MRS advances* **2018**, *3*, 3135-3141.
24. Uprety, P.; Wang, C.; Koirala, P.; Sapkota, D.; Ghimire, K.; Junda, M.; Collins, R. Application of Optical Hall Effect to PV Relevant Materials. *Bulletin of the American Physical Society* **2018**, *63*.
25. Sapkota, D.R.; Pradhan, P.; Irving, R.; Grice, C.R.; Phillips, A.B.; Heben, M.J.; Marsillac, S.; Podraza, N.J.; Collins, R.W. Evaluation of $CuInSe_2$ Materials and Solar Cells Co-evaporated at Different Rates Based on Real Time Spectroscopic Ellipsometry Calibrations. In Proceedings of 2021 IEEE 48th Photovoltaic Specialists Conference (PVSC); pp. 0451-0458.
26. Uprety, P.; Wang, C.; Koirala, P.; Sapkota, D.R.; Ghimire, K.; Junda, M.M.; Yan, Y.; Collins, R.W.; Podraza, N.J. Optical Hall Effect of PV Device Materials. *IEEE Journal of Photovoltaics* **2018**, *8*, 1793-1799, doi:10.1109/JPHOTOV.2018.2869540.
27. Sapkota, D.R.; Pradhan, P.; Koirala, P.; Ramanujam, B.; Grice, C.; Irving, R.; Heben, M.J.; Collins, R.W. Optimization of the CuInSe$_2$ Absorber for the Bottom Cell of a Polycrystalline Thin Film Tandem Solar Cell. *Bulletin of the American Physical Society* **2020**, *65*.
28. Sapkota, D.R. Characterization and Optimization of CuInSe2 Solar Cells Applicable for Tandem Devices. University of Toledo, 2022.
29. Orgassa, K.; Schock, H.W.; Werner, J. Alternative back contact materials for thin film Cu (In,Ga)Se_2 solar cells. *Thin Solid Films* **2003**, *431*, 387-391.
30. Minemoto, T.; Matsui, T.; Takakura, H.; Hamakawa, Y.; Negami, T.; Hashimoto, Y.; Uenoyama, T.; Kitagawa, M. Theoretical analysis of the effect of conduction band offset of window/CIS layers on performance of CIS solar cells using device simulation. *solar Energy Materials and solar Cells* **2001**, *67*, 83-88.
31. Pradhan, P.; Aryal, P.; Ibdah, A.-R.; Koirala, P.; Li, J.; Podraza, N.J.; Rockett, A.A.; Marsillac, S.; Collins, R.W. Effect of molybdenum deposition temperature on the performance of $CuIn_{1-x}Ga_xSe_2$ solar cells. In Proceedings of 2015 IEEE 42nd Photovoltaic Specialist Conference (PVSC); pp. 1-4.
32. Aryal, P. *Optical and photovoltaic properties of copper indium-gallium diselenide materials and solar cells*; The University of Toledo: 2014.

 doi:10.20944/preprints202305.1203.v1

33. Fujiwara, H.; Koh, J.; Rovira, P.; Collins, R. Assessment of effective-medium theories in the analysis of nucleation and microscopic surface roughness evolution for semiconductor thin films. *Physical Review B* **2000**, *61*, 10832.